AGU PUBLICATIONS

Geophysical Research Letters

RESEARCH LETTER
10.1002/2014GL061963

Key Points:
- An interferometric-TOA LF 3-D Lightning Mapping Array was designed and applied
- Mapped and measured stepped and dart leaders from both IC and CG flashes
- Imaged entire LF structure of different flashes which is similar as VHF maps

Correspondence to:
S. A. Cummer,
cummer@ee.duke.edu

Citation:
Lyu, F., S. A. Cummer, R. Solanki, J. Weinert, L. McTague, A. Katko, J. Barrett, L. Zigoneanu, Y. Xie, and W. Wang (2014), A low-frequency near-field interferometric-TOA 3-D Lightning Mapping Array, *Geophys. Res. Lett.*, *41*, doi:10.1002/2014GL061963.

Received 22 SEP 2014
Accepted 3 NOV 2014
Accepted article online 6 NOV 2014

A low-frequency near-field interferometric-TOA 3-D Lightning Mapping Array

Fanchao Lyu[1], Steven A. Cummer[1], Rahulkumar Solanki[1], Joel Weinert[1], Lindsay McTague[1], Alex Katko[1,2], John Barrett[1], Lucian Zigoneanu[1,3], Yangbo Xie[1], and Wenqi Wang[1]

[1]Electrical and Computer Engineering Department, Duke University, Durham, North Carolina, USA, [2]Now at the Metamaterials Commercialization Center, Intellectual Ventures in Bellevue, Bellevue, WA, USA, [3]Now at Portland Technology Development, Intel Corp., Hillsboro, Oregon, USA

Abstract We report on the development of an easily deployable LF near-field interferometric-time of arrival (TOA) 3-D Lightning Mapping Array applied to imaging of entire lightning flashes. An interferometric cross-correlation technique is applied in our system to compute windowed two-sensor time differences with submicrosecond time resolution before TOA is used for source location. Compared to previously reported LF lightning location systems, our system captures many more LF sources. This is due mainly to the improved mapping of continuous lightning processes by using this type of hybrid interferometry/TOA processing method. We show with five station measurements that the array detects and maps different lightning processes, such as stepped and dart leaders, during both in-cloud and cloud-to-ground flashes. Lightning images mapped by our LF system are remarkably similar to those created by VHF mapping systems, which may suggest some special links between LF and VHF emission during lightning processes.

1. Introduction

Very high frequency (VHF) lightning flash imaging is an important technique for the study of lightning processes. VHF imaging provides a description of the extent of intracloud discharge (IC) channels as well as the in-cloud development of cloud-to-ground discharges (CG), both of which are typically unobservable using photographic measurements. After the first detailed discussion of VHF radio pictures of IC flashes [*Proctor*, 1981] and CG flashes [*Proctor et al.*, 1988] by VHF time of arrival (TOA) system, more lightning mapping systems operating in VHF frequency range were designed and developed. These included both narrowband [*Rhodes et al.*, 1994] and wideband [*Shao et al.*, 1996; *Stock et al.*, 2014] VHF interferometry systems, as well as systems utilizing time of arrival (TOA) techniques [*Rison et al.*, 1999; *Thomas et al.*, 2004], and application by other researchers [e.g., *Sun et al.*, 2013]. The Lightning Mapping Array (LMA), the most widely used VHF TOA system in United States in lightning-related studies, was designed and developed by New Mexico Tech to use GPS time synchronization, allowing it to locate 3-D VHF sources and therefore map channel development during IC and CG flashes [*Rison et al.*, 1999; *Thomas et al.*, 2004].

Lightning discharges produce wideband electromagnetic signals, thus allowing for the development of other location networks that use different signal frequencies. Lightning emissions at different frequencies are produced by different lightning processes, so flash imaging at frequencies other than VHF would be a valuable tool for examining lightning processes. Currently common are lightning location systems based on very low frequency (VLF) and low-frequency (LF) signals. However, most LF systems operate as 2-D ground point location networks, e.g., National Lightning Detection Network (NLDN) [*Cummins et al.*, 1998] and Los Alamos Sferic Array [*Smith et al.*, 2002], or thunderstorm tracking networks, e.g., Lightning Detection Network deployed in Europe [*Betz et al.*, 2004] and Earth Networks Total Lightning Network in the U.S. [*Liu and Heckman*, 2011], with no ability to measure flash extent or detailed step processes during the development of flashes. Recent work has demonstrated LF 3-D mapping of some discrete lightning pulses. A 7-station VLF/LF sensor (1 Hz to 400 kHz) TOA network (Huntsville Alabama Marx Meter Array (HAMMA)) with baseline of 10–15 km deployed in Huntsville, AL, [*Bitzer et al.*, 2013] records LF pulses in ~1 s record (~100 ms pretrigger) that are manually parsed and located using TOA. Although HAMMA did not locate as many sources (a few tens to a few hundreds) as North Alabama LMA (NALMA), the relationship between HAMMA and NALMA is well correlated [*Bitzer et al.*, 2013]. Another similar 11-station VLF/LF (500 Hz to 500 kHz) TOA location network (BOLT) was deployed to study the initiation of IC events following narrow bipolar

events (NBE), the speed of upward leaders initiated by positive NBE at different altitudes is estimated, and the extent of an IC flash is largely mapped [*Wu et al*., 2014]. However, all of these LF networks measure the triggered strong impulsive signals or the postprocessed time of signal peaks. Although this allows for the location of some discrete lightning pulses, it does not generate enough points to sufficiently image a flash. Furthermore, such networks may not do well at imaging the development of continuous LF sources, especially fast processes, such as dart leaders, which appear as quasi-continuous signal bursts.

In this work we report on the design and deployment of an LF near-field interferometric-TOA 3-D Lightning Mapping Array (LFI-LMA). LF magnetic signals were recorded continuously with a sensor that mixes B(t) and dB/dt responses to emphasize continuous fast pulse emissions, which are preferred by interferometry. Instead of using the time of a solitary LF pulse, the technique of cross correlation of continuous signals used by interferometry is applied to automatically calculate the arrival time differences of sources in a fixed time window. The TOA location method [*Thomas et al*., 2004] is then applied to these time differences to determine the source locations. This hybrid processing method images both impulsive and continuous emissions and is thus capable of imaging both discrete (stepped) and continuous (dart) leader processes. The resulting images are remarkably similar to those of VHF LMA, indicating that LF and VHF emissions are tightly linked in lightning processes, despite differences in frequency and time scale of approximately 3 orders of magnitude.

2. Instrumentation and Data Processing

The current network was composed of five LF stations (named here as Duke, Hudson, PS1, PS2, and PS4), with interstation separations of 15–20 km. Each station was equipped with two orthogonal LF magnetic field sensors, a data acquisition system and a GPS receiver. All sensors have the same bandwidth of 1–400 kHz, with a dB/dt response from 1 to 100 kHz and a flat (B) response from 100 to 250 kHz. This sensor response helps boost the signal received from fast continuous emissions. The polarity of discharge can be determined by the Bphi and Br component when the location of the discharge is known. These signals were recorded continuously with a sampling rate of 1 MHz. All stations were synchronized by GPS, and correction of GPS absolute time between stations is done in postprocessing with arrival time of NLDN reported return strokes (RSs) more than 500 km from the network to ensure submicrosecond absolute time accuracy. Among all these five stations, three (PS1, PS2, and PS4) are mobile and were operated in parked cars. As these systems utilize the 12 V DC power supplied by the vehicle, the network is very flexible and adaptable and not dependent on local power availability.

The data processing employs a hybrid interferometric-TOA technique. A simple VHF interferometry array is usually composed by at least three sensors deployed with a baseline comparable to the wavelength of measuring signal frequency (thus a few meters for VHF) to measure phase or time differences across the sensors. Our LF system (wavelength at 100 kHz is 3 km) employs sensor spacing of a few wavelengths, and thus, interferometric processing is feasible. Hence, we perform data processing in similar manners as broadband interferometry [*Shao et al*., 1996; *Stock et al*., 2014], with time difference between each pair of stations being determined via cross correlation. However, there is an essential difference between VHF interferometry and our system in the distance of sources in relation to wavelength. VHF sources are usually hundreds to thousands of wavelengths away from VHF sensor array (and thus in the far field of the array), allowing for the precise measurement of the arrival angle to the source from the phase or time difference across the array. However, since LF sources are only a few wavelengths away (and thus in the near field of the array), the source arrival angle cannot be measured from time or phase differences. As a result, the TOA approach is applied to calculate the source location from the measured time differences across stations.

During the cross-correlation process between signals from each two stations, a 350 μs time window and a short sliding step of 50 μs are applied. The data in that window are upsampled to 10 MHz to give 100 ns resolution, and two magnetic components are rotated inside each time window to give a signal maximum amplitude waveform that will be used in cross correlation. The choice of 350 μs window length is somewhat arbitrary but is found to be effective. The window should (1) be at least twice longer than the maximum time interval between each pair of stations (which is 75 μs), (2) contain enough signal energy for cross correlation, and (3) not be so long that there are too many source locations. Other window options could be used, and might improve certain features, but we use 350 μs to achieve a more comprehensive image in the present analysis. For each window, an event is identified when the maximum normalized cross-correlation

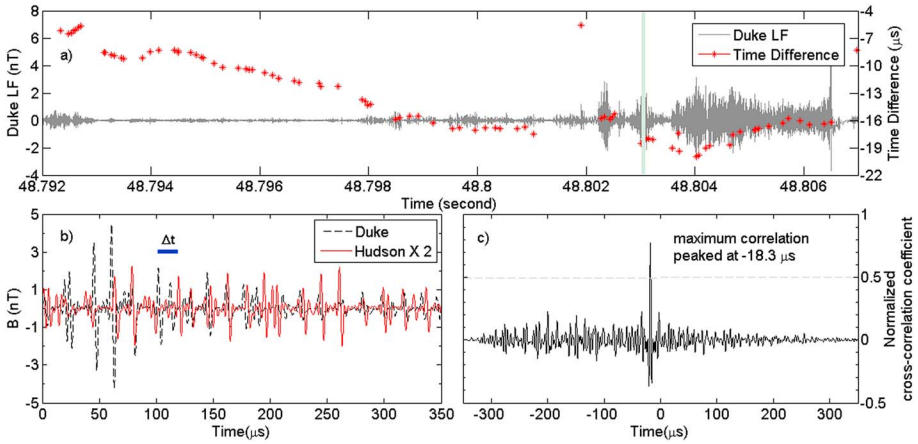

Figure 1. Cross-correlation results between LF signals from two different sensors (Duke and Hudson). (a) Overview of LF signal and time difference within a period (with normalized cross-correlation coefficient ≥0.5). (b) Interpolated (10X) LF signal from two sensors within a particular time window marked by the grey bar in Figure 1a; windowed data are upsampled to 10 MHz to give 100 ns resolution in cross correlation, and time difference is indicated by the blue bar. (c) Normalized cross-correlation coefficient of signals shown in Figure 1b, with maximum correlation coefficient maximum at -18.3 μs; the dashed grey line shows the threshold of the cross-correlation coefficient.

coefficient ≥0.5 is found, with the time at the center of that window being used as the source time (resulting in a time uncertainty that is less than 175 μs). When multiple peaks above 0.5 are found (which is rarely), only the maximum is kept. We note that this time uncertainty has very little effect on maps of the whole flash structures or on the propagation speed estimation of leaders. The relatively short window sliding step is also allows the mapping of more continuous processes. Note that large peak signals could appear multiple times in successive windows because of the small window shift; these duplicate locations are removed as described later.

Figure 1 shows an example of cross-correlation performance between LF signals from the Duke and Hudson sensors. As shown in Figures 1a and 1b, it may seem redundant and challenging to find every pulse's time difference without ambiguity. However, windowed time difference by cross correlation and the short sliding step are efficient and useful for lightning step mapping, as seen in Figure 1c and demonstrated in following section. Location results related to the signals shown in Figure 1 can be found in Figure 3 in the following section. Again, our aim is not to demonstrate the optimality of these particular processing parameters but instead to show that reasonable parameters generate high quality and scientifically valuable lightning flash images.

The TOA location-finding method is then applied to the computed time differences. A source arrival time database in horizontal area of -50 50 km $\times -50$ 50 km and height of 0 18 km is prebuilt, with 80 m horizontal resolution and 200 m vertical resolution, which is consistent with location accuracy as discussed below. Source location is found by finding the minimum χ^2 on arrival times between database and results of cross correlation. In our definition, $\chi^2 = \frac{\Sigma(\Delta T_i - \Delta t_i)^2}{(N-1)\tau^2}$, $(\mathrm{i} = 1, \ldots, \mathrm{N}-1)$, where ΔT is the time difference from the database, Δt is the time difference from cross correlation, N is number of sensors, and τ is the typical time accuracy. The accuracy τ is determined from the distribution of the residual value of time differences between database and cross-correlation calculations ($\tau \sim \sqrt{\Sigma(\Delta T_i - \Delta t_i)^2}$). From observation, nearly 88% of all located points correspond to τ of less than 400 ns (with spatial accuracy of 120 m). As a result, a typical time accuracy of 400 ns is assumed in our system, and only points with minimum χ^2 less than 1 are kept as reliable locations. Postprocessing is applied to exclude doubly located sources because of the overlap of pulses in successive windows.

The network location error is estimated by simulation, similar to *Bitzer et al.* [2013]. When considering near-field measurements, the time error mainly relates to timing accuracy. In our case ($\tau \leq 400$ ns), assuming a measuring time error of ±400 ns, a horizontal error of less than 200 m (with best error of ~50 m), and a height error of less than 250 m (with best error of ~100 m) at an altitude of 5 km is achieved inside the network.

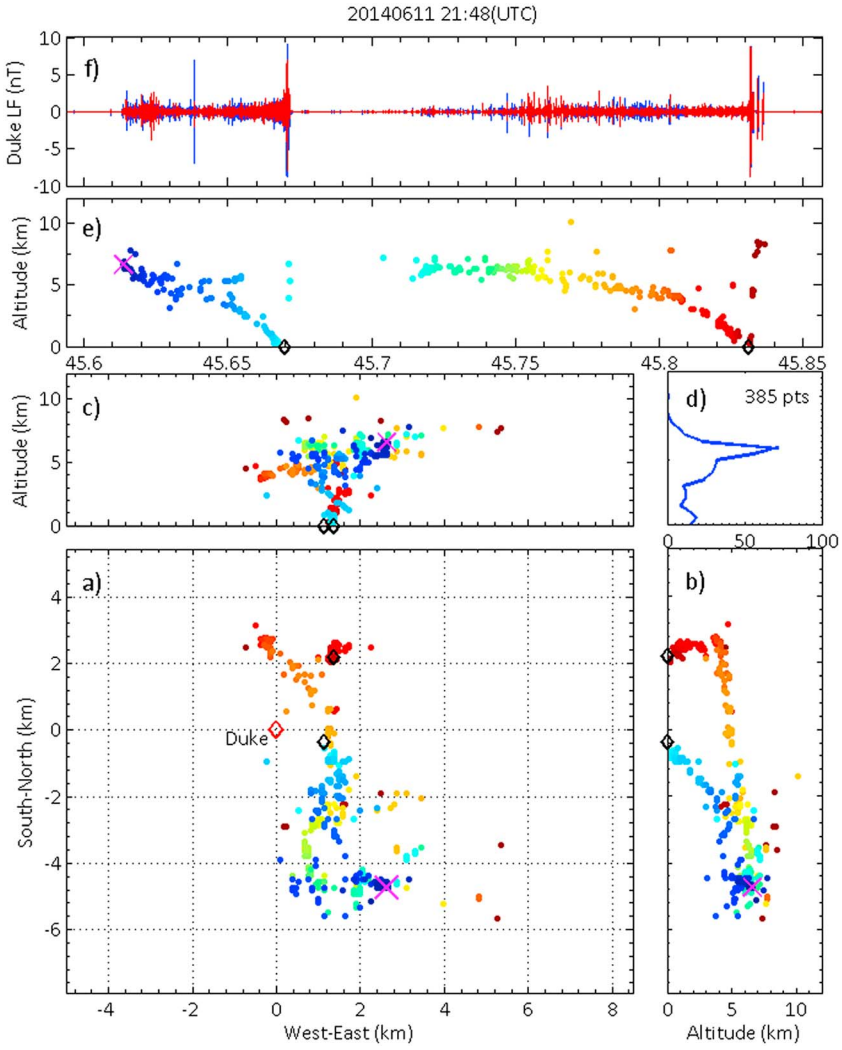

Figure 2. Image of a compact CG flash and LF signal. (a) Plan view of the located LF sources, Duke sensor location (red diamond; other sensors are outside the limits), NLDN reported stroke location (black diamond), and initiation point of the flash (magenta cross). (b) Vertical view of LF sources from direction of west to east. (c) Vertical view of LF sources from direction of south to north. (d) Total source points (385 points) located and the height distribution. (e) LF sources height versus time (second scale) during the flash. (f) LF signal measured by Duke sensor, with different colors showing orthogonal magnetic LF signals with same time coordination of Figure 2e.

However, we should note here that among all located sources, the points having minimum χ^2 less than 0.4 often account for up to 85% of the total points, meaning that better location performances than these typical cases can be achieved. Furthermore, the good location results can also be verified using the following well-resolved flash channel structure, the self-consistent location results on CG strokes from same channel (less than 150 m discrepancy), and stroke location comparison with NLDN.

3. Results

During a 1 h field observation on 11 June 2014, a total of more than 3600 events were reported by NLDN within 30 km of the network center, with hundreds of flashes. Here we show two examples to demonstrate the capabilities of the LFI-LMA. The system is able to resolve all types of leader activities, including stepped leader and dart leader during IC flashes as well as CG flashes. In the first case, we show a compact CG flash with clear downward leaders and two distinct ground channels. The second case shows an IC flash and a CG flash that occurred simultaneously but spatially separated. The full extent of the lightning flash and different flash processes were clearly mapped and examined.

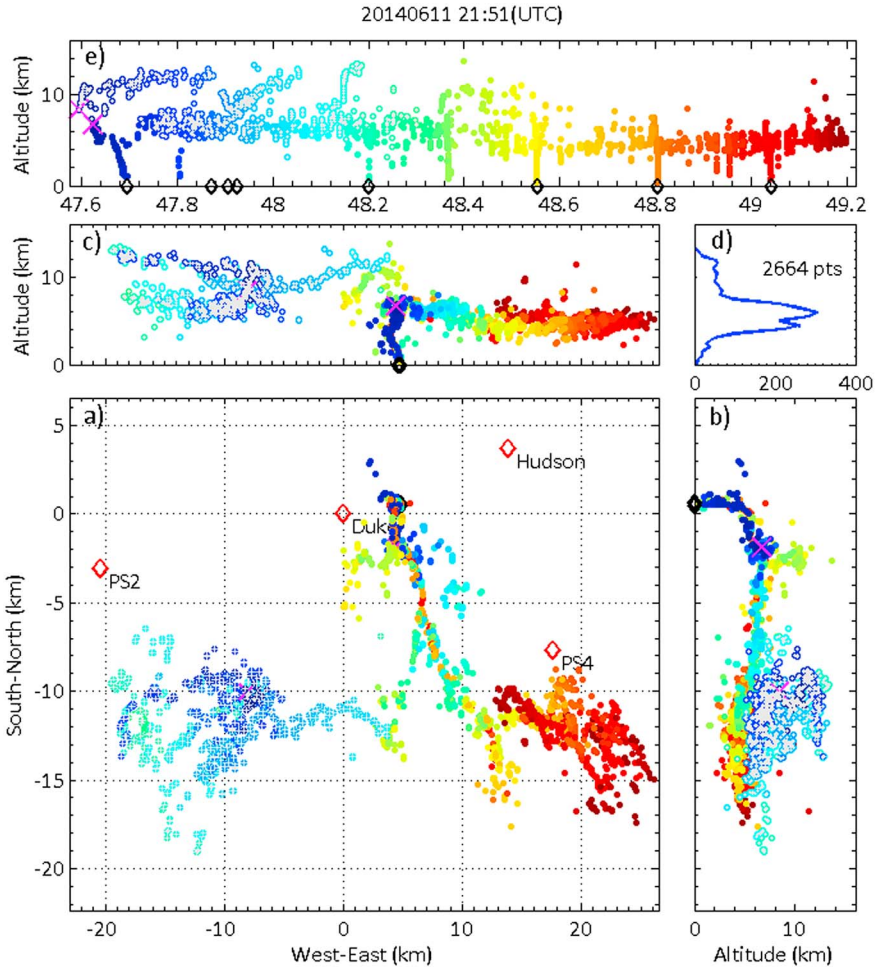

Figure 3. Image of simultaneous IC and CG flashes (signs have the same meaning as those in Figure 2, Duke and Hudson indicate the two immobile stations, and PS2 and PS4 indicate the two of the mobile stations), with two magenta crosses, plot the initiation of IC and CG flashes, respectively.

3.1. Compact CG Flash With Two Different Channels

Figure 2 shows the Duke LF signal and the processed 3-D image of a very compact negative CG flash that occurred at 21:48:45 UTC. The flash starts at 45.614 s and contains two RSs separated by 164 ms, which were reported by NLDN to have peak currents of 15 kA and 11 kA, respectively. As shown in the LF signal plot, both CG strokes have detectable leader LF radiation during their descent. A total of 385 LF source points were located by the LFI-LMA, with peak in the altitude distribution at 5–7 km. The first leader process initiated at 6.6 km above ground level (agl) at 45.614 s. The leader then divided into two branches at about 4 km agl, with one moving horizontally and stopping at 45.655 s and the other propagating downward continuously for 56.6 ms with an average downward propagation speed of 1.2×10^5 m/s until the first RS occurred. After the first RS, LF source activity ceases almost entirely during the following 33 ms. The second RS begins in almost the same region as the first, at 45.704 s at 7.1 km agl. After another 10 ms, the LF sources become continuous and follow the previous leader channel for the next 60 ms. The leader then splits from the old channel to ground and follows a different horizontal branch that previously stopped at 45.655 s during the development of the first leader. This leader then branches, with one continuing horizontally and the other following a downward path with average downward propagation speed of about 0.6×10^5 m/s and becoming the second ground stroke.

This is a good example of the type of flash that has been referred to as a "new channel flash" [*Valine and Krider*, 2002]. As shown in 3-D image, the LFI-LMA clearly resolve the in-cloud leader structure and the stepped leader development in two different strokes. Leaders propagating in the same in-cloud channel and

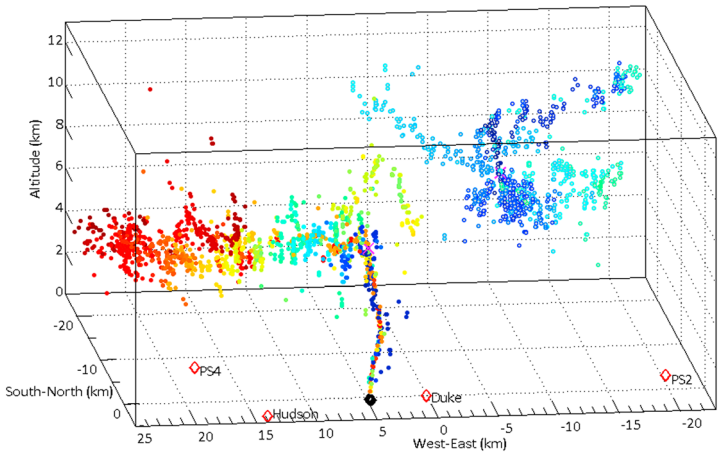

Figure 4. The 3-D view of the simultaneous IC and CG flashes shown in Figure 3. No clear spatial connection can be seen from the 3-D view. Different layers for IC and CG flashes and the decent channel of CG flash are imaged.

those extending to new channels were also well mapped. The stepped leader downward propagation speeds are consistent with other reported speeds. The location differences of the two ground strokes between LFI-LMA and NLDN are 197 m (first RS) and 119 m (second RS). In light of known NLDN location uncertainties [*Nag et al*., 2011], the results of LFI-LMA and NLDN are consistent, which also verify the capability of LFI-LMA systems in measuring lightning development.

3.2. Simultaneous IC and CG Flashes

Figures 3 and 4 show LFI-LMA images for two simultaneous, nearly overlapping, but probably spatially distinct IC and CG flashes that together last about 1.6 s. As shown in Figure 3, a total of more than 2600 LF sources were located. The IC sources are plotted with grey cross on color points for better discrimination. Similar to the previous example, continuous in-cloud leader structure and extension are well resolved. This example also show that both stepped leaders and dart leaders in both IC and CG flashes are mapped.

The typical bilevel structure IC begins with a clear negative upward stepped leader starting at 47.595 s at 8.5 km agl, with an average upward speed of 2.5×10^5 m/s, consistent with previous studies by VHF interferometer [*Shao and Krehbiel*, 1996], VHF TOA system [*Proctor*, 1981; *Behnke et al*., 2005], and VLF/LF 3-D TOA location system [*Bitzer et al*., 2013; *Wu et al*., 2014]. After IC initiation, LF sources were detected in two altitude layers separated by about 4–5 km. An upward dart leader at 48.15 s with estimated upward speed of 1.9×10^6 m/s propagating from a lower charge region to an upper region was mapped, indicating a charge transfer between different charge layers through a previously built in-cloud channel. The IC flash concluded at about 48.3 s.

Approximately 29.5 ms after IC initiation, a negative CG flash started at 47.625 s, with initial breakdown pulses lasting about 3 ms, and LF sources decreasing from 6.7 km to 4.9 km agl. In the following 37 ms, a negative stepped leader propagated downward continuously from 5.8 km agl until first RS occurred, with average downward speed of 1.6×10^5 m/s. During next 0.3 s, the CG and IC flashes developed simultaneously but were spatially separated, as indicated from Figure 4. In this window, LF sources from the IC flash dominated the received signal, and thus, three RSs reported by NLDN are not mapped. However, seven clear dart leaders following exactly the same channel established by the previous stepped leader and first RS were imaged. Three of these seven RSs were not reported by NLDN and are seen at 48.36 s, 48.92 s, and 48.96 s. The estimated dart leader downward speed ranges from 0.8 to 2×10^6 m/s, about an order of magnitude faster than the stepped leader in previous example or other studies [*Rakov and Uman*, 2003], and comparable to reported dart leader [*Stolzenburg et al*., 2013].

All of the located dart leaders before each RS share the same path to ground, as expected. The largest distance between different RSs located by LFI-LMA is 114 m, while the largest distance of those reported by NLDN is 322 m. Location differences between LFI-LMA and NLDN range from 63 m to 323 m. Considering the

larger distance of RSs reported by NLDN (322 m of NLDN to 114 m of our system) and NLDN location uncertainty [*Nag et al*., 2011], results from LFI-LMA and NLDN are consistent.

It is important to note that the same data and processing are able to map both stepped leaders and dart leaders with high fidelity, provided that other simultaneous lightning processes do not swamp the signal. Dart leaders in particular have proven challenging to capture with other lightning TOA imaging systems [*Cummins and Murphy*, 2009], especially LF systems. In addition to lightning mapping, thunderstorm charge layers related to particular lightning can also be inferred from the LF sources distribution. As shown in Figure 3d (also in Figure 2d), LF sources were located in two main different layers, at 4–5 km and 5–7 km, respectively. These two layers show main negative charge region for the negative CG and IC. A third, higher layer at 9–12 km indicates an upper positive charge region related to the IC. The height distribution indicated by LF sources is also consistent with conceptual model of charge structure of thunderstorms [*Stolzenburg et al*., 1998] and charge layers separation indicated by LMA images [*Rison et al*., 1999]. One interesting result of this work is that images mapped by LFI-LMA are incredibly similar (aside from the easier detection of dart leaders) to those mapped by VHF systems (such as LMA). The identical appearance of images measured by signals with frequency difference of 3 orders of magnitude may suggest some special link between LF and VHF emissions in leaders.

4. Conclusions and Discussion

In this paper, we report the development and demonstration of an LF near-field interferometric-TOA 3-D Lightning Mapping Array (LFI-LMA). The deployment and operation of system is simple, portable, and even real-time reconfigurable, although continuous recording is data intensive. Compared to the previous LF lightning detection systems [*Cummins et al*., 1998; *Smith et al*., 2002; *Betz et al*., 2004; *Bitzer et al*., 2013; *Wu et al*., 2014], a five station LFI-LMA can detect thousands of points per flash and completely image entire lightning flash structure. More importantly, we easily see and image not only the extent of different flashes but also some important lightning processes, i.e., step leader and dart leader, as well as other continuous lightning processes during both IC and CG flashes. As illustrated in two examples, step leader in a typical bilevel IC transfers negative charge upward to the upper positive charge region, and IC dart leader starts from the position of previous breakdowns in lower negative charge region and ends at the position of former breakdowns in upper positive charge region, agree with VHF studies on *K* processes [*Shao and Krehbiel*, 1996; *Akita et al*., 2010]. While step leaders in CGs may branch in different directions before RS occur. And then, a new leader could create another path to ground as new step leader or start from previous breakdown position in negative charge region and follow the previous RS channel to ground as dart leaders.

One remarkable result is that images produced by LFI-LMA show lightning flash images that are incredibly similar to LMA images from VHF emissions. Similar observations from HAMMA also showed correlated results between LF sources and LMA reports, even with fewer located LF sources than LMA [*Bitzer et al*., 2013]. The widely different measuring frequencies of LF and VHF imaging systems (about 1000X difference) mean that widely different time scales and spatial scales are being probed by each system. The similarity indicates special ties between the physics of lightning processes despite the different scales. VHF emissions are thought to image the leader corona, which relate to the ionization or breakdown into virgin air, while at LF, we see charge motion from the leader steps themselves. Apparently, these two processes are intimately linked together, and they may happen accordingly during the lightning leader processes. As a result, we usually see both LF pulses and VHF emission at the same time during lightning leader processes from measurements, and we may not see the location differences even on relatively short time scale.

Acknowledgments
The authors would like to acknowledge support from the National Science Foundation Dynamic and Physical Meteorology program through grant ATM-1047588 and the DARPA Nimbus program through grant HR0011-10-1-0059. We would like to thank Jeannie Chung for participating in the field observations and Adam Konneker for evaluating the writing of this paper. LF radio data for the two events analyzed here are available by request (cummer@ee.duke.edu), and the processing details are described fully in the manuscript.

The Editor thanks Robert Holzworth and Xiushu Qie for their assistance in evaluating this paper.

References

Akita, M., Y. Nakamura, S. Yoshida, T. Morimoto, T. Ushio, Z. Kawasaki, and D. Wang (2010), What occurs in K process of cloud flashes?, *J. Geophys. Res.*, *115*, D07106, doi:10.1029/2009JD012016.

Behnke, S. A., R. J. Thomas, P. R. Krehbiel, and W. Rison (2005), Initial leader velocities during intracloud lightning: Possible evidence for a runaway breakdown effect, *J. Geophys. Res.*, *110*, D10207, doi:10.1029/2004JD005312.

Betz, H. D., K. Schmidt, P. Oettinger, and M. Wirz (2004), Lightning detection with 3-D discrimination of intracloud and cloud-to-ground discharges, *Geophys. Res. Lett.*, *31*, L11108, doi:10.1029/2004GL019821.

Bitzer, P. M., H. J. Christian, M. Stewart, J. Burchfield, S. Podgorny, D. Corredor, J. Hall, E. Kuznetsov, and V. Franklin (2013), Characterization and applications of VLF/LF source locations from lightning using the Huntsville Alabama Marx Meter Array, *J. Geophys. Res. Atmos.*, *118*, 3120–3138, doi:10.1002/jgrd.50271.

Cummins, K. L., and M. J. Murphy (2009), An overview of lightning location systems: History, techniques, and data uses, with an in-depth look at the U. S. NLDN, *IEEE Trans. Electromagn. Compat.*, *51*, 499–518.

Cummins, K. L., M. J. Murphy, E. A. Bardo, W. L. Hiscox, R. Pyle, and A. E. Pifer (1998), Combined TOA/MDF technology upgrade of U. S. National Lightning Detection Network, *J. Geophys. Res.*, *103*, 9035–9044, doi:10.1029/98JD00153.

Liu, C., and S. Heckman (2011), Using total lightning data in severe storm prediction: global case study analysis from North America, Brazil and Australia, 2011 International Symposium on Lightning Protection (XI SIPDA), pp. 20–24.

Nag, A., et al. (2011), Evaluation of U.S. National Lightning Detection Network performance characteristics using rocket-triggered lightning data acquired in 2004–2009, *J. Geophys. Res.*, *116*, D02123, doi:10.1029/2010JD014929.

Proctor, D. E. (1981), VHF radio pictures of cloud flashes, *J. Geophys. Res.*, *86*, 4041–4071, doi:10.1029/JC086iC05p04041.

Proctor, D. E., R. Uytenbogaardt, and B. M. Meredith (1988), VHF radio pictures of lightning flashes to ground, *J. Geophys. Res.*, *93*, 12,683–12,727, doi:10.1029/JD093iD10p12683.

Rakov, V. A., and M. A. Uman (2003), *Lightning Physic and Effects*, pp. 687, Cambridge Univ. Press, Cambridge, U. K.

Rhodes, C. T., X. M. Shao, P. R. Krehbiel, R. J. Thomas, and C. O. Hayenga (1994), Observations of lightning phenomena using radio interferometry, *J. Geophys. Res.*, *99*, 13,059–13,082, doi:10.1029/94JD00318.

Rison, W., R. J. Thomas, P. R. Krehbiel, T. Hamlin, and J. Harlin (1999), A GPS-based three-dimensional lightning mapping system: Initial observations in central New Mexico, *Geophys. Res. Lett.*, *26*, 3573–3576, doi:10.1029/1999GL010856.

Shao, X. M., and P. R. Krehbiel (1996), The spatial and temporal development of intracloud lightning, *J. Geophys. Res.*, *101*, 26,641–26,668, doi:10.1029/96JD01803.

Shao, X. M., D. N. Holden, and C. T. Rhodes (1996), Broad band radio interferometry for lightning observations, *Geophys. Res. Lett.*, *23*, 1917–1920, doi:10.1029/96GL00474.

Smith, D., K. Eack, J. Harlin, M. Heavner, A. Jacobson, R. Massey, X. Shao, and K. Wiens (2002), The Los Alamos Sferic Array: A research tool for lightning investigations, *J. Geophys. Res.*, *107*(D13), 4183, doi:10.1029/2001JD000502.

Stock, M. G., M. Akita, P. R. Krehbiel, W. Rison, H. E. Edens, Z. Kawasaki, and M. A. Stanley (2014), Continuous broadband digital interferometry of lightning using a generalized cross-correlation algorithm, *J. Geophys. Res. Atmos.*, *119*, 3134–3165, doi:10.1002/2013JD020217.

Stolzenburg, M., W. D. Rust, and T. C. Marshall (1998), Electrical structure in thunderstorm convective regions: 3. Synthesis, *J. Geophys. Res.*, *103*, 14,097–14,108, doi:10.1029/97JD03545.

Stolzenburg, M., T. C. Marshall, S. Karunarathne, N. Karunarathna, T. A. Warner, and R. E. Orville (2013), Stepped-to-dart leaders preceding lightning return strokes, *J. Geophys. Res. Atmos.*, *118*, 9845–9869, doi:10.1002/jgrd.50706.

Sun, Z. L., X. S. Qie, M. Y. Liu, D. J. Cao, and D. F. Wang (2013), Lightning VHF radiation location system based on short-baseline TDOA technique-validation in rocket-triggered lightning, *Atmos. Res.*, *129–130*, 58–66, doi:10.1016/j.atmosres.2012.11.010.

Thomas, R., P. Krehbiel, W. Rison, S. Hunyady, W. Winn, T. Hamlin, and J. Harlin (2004), Accuracy of the lightning mapping array, *J. Geophys. Res.*, *109*, D14207, doi:10.1029/2004JD004549.

Valine, W. C., and E. P. Krider (2002), Statistics and characteristics of cloud-to-ground lightning with multiple ground contacts, *J. Geophys. Res.*, *107*(D20), 4441, doi:10.1029/2001JD001360.

Wu, T., S. Yoshida, T. Ushio, Z. Kawasaki, and D. H. Wang (2014), Lightning-initiator type of narrow bipolar events and their subsequent pulse trains, *J. Geophys. Res. Atmos.*, *119*, 7425–7438, doi:10.1002/2014JD021842.